$$\bar{\varepsilon}_{G,trans} = 0.59 C_1^{1.5} \left(\frac{\rho_G^{0.96} \sigma_s^{0.12}}{\rho_L} \right)^{0.5}, \tag{2.22}$$

where the coefficient C_1 assumes the value for churn-turbulent flow, and

$$U_{G,trans} = \frac{1}{2.84} \frac{\sigma_s^{0.12}}{\rho_G^{0.04}} \bar{\varepsilon}_{G,trans} (1 - \bar{\varepsilon}_{G,trans}). \tag{2.23}$$

These formulas were derived from data over the following ranges: $\sigma_s = 0.024 - 0.073$ N/m, $\rho_L = 685 - 1460$ kg/m^3, $\rho_G = 0.16 - 13.0$ kg/m^3. The holdup correlation was compared to high-pressure pilot plant data from other investigators as well as the data used in its own derivation. For experimental holdup values less than 0.5, the relative error was less than 10%, slightly better than the Wilkinson correlation. The error increased rapidly at higher holdup values, however, requiring the adjustments described earlier in conjunction with Eq. 2.13.

Reilly *et al.* (1994) and Krishna *et al.* (1994) also found in experiments that increasing ρ_G extended the stability of the bubbly flow regime to higher $\bar{\varepsilon}_{G,trans}$. Krishna and Ellenberger (1996) found Eqs. 2.22 and 2.23 to be more accurate than Eq. 2.21 for a variety of gas-liquid systems. They also found that a theoretical criterion by Biesheuvel and Gorissen (1990) for the instability of homogeneous bubbly flows overpredicted $\bar{\varepsilon}_{G,trans}$ and should be considered to be an upper limit on the gas volume fraction at transition. In actual bubbly flows, destabilizing influences (such as an imperfect gas distribution) will lead to an earlier transition to churn-turbulence than the criterion predicts. They recommended further study of the influence of the liquid phase properties on $\bar{\varepsilon}_{G,trans}$ and $U_{G,trans}$.

2.3. Mathematical Multiphase Flow Models

Until recently, multiphase measurement methods have only been able to produce time-averaged and volume-averaged quantities that could not reveal instantaneous flow structures. Tomographic methods, such as the electrical impedance method discussed in the next three chapters, have the potential to provide the instantaneous three-dimensional phase distributions and flow fields needed to understand dynamic flows. The alternative to experimentation, multiphase mathematical modeling, suffers from the current inability to determine three-dimensional phase and velocity distributions. In practice, experimental observations of $\varepsilon_G(r,\theta,z)$ must be used as a starting point, or simplified one-dimensional predictive models must be used. A comprehensive review of hydrodynamic bubble-column models is given by Shah and Deckwer (1983), including information on bubbly flows, flow regimes, averaged liquid flow patterns, bubble size populations, and bubble coalescence and breakup. Useful tools for bubble-column reactor design can also be found in Deckwer and Schumpe (1993).

Two models of gas volume fraction distribution and three models for phase velocity are discussed in this section; one of the latter can be applied to a wide variety of two-phase systems. These have been derived from first principles and substantiated by empirical data and correlations. A starting point for many models of vertical multiphase flows is the two-fluid model. This model treats the multiphase fluid as a continuum in which the equations of conservation of mass and momentum and the first and second laws of thermodynamics may be written for each phase in the flow. The continuum model implies that the phases can overlap one another in space, and that phase changes and chemical reactions can alter the amount of mass in each phase (but not the total mass in the flow). By averaging terms in the equations over time, space, or other appropriate variables, the two-fluid model may be reduced to more manageable forms, such as the one-dimensional two-phase bubble-column model used to derive Eqs. 2.1 through 2.10. The one-dimensional two-phase bubble-column model assumes steady-state, axisymmetric flow that is fully developed and involves no end effects. The largest source of uncertainty in the two-fluid model (even in its simplified one-dimensional two-phase form) is the stress tensor, which has been simplified in different ways with varying degrees of success (Kumar *et al.*, 1994).

2.3.1. One-Dimensional Gas Volume Fraction Models

In the early paper by Zuber and Findlay (1965), a general expression was derived for the area-averaged gas volume fraction, $\langle \varepsilon_G \rangle$, in one-dimensional, dispersed two-phase flow. This expression accounted for nonuniform flows and concentration distributions and included the effects of local relative velocities between the phases. Their iterative formulation applied to any two-phase flow regime with no heat or mass transfer:

$$\langle \varepsilon_G \rangle = \frac{U_G / U_m}{C_0 + C_1} , \tag{2.24}$$

where U_m is the superficial velocity of the mixture. The effects of the local relative velocities between phases are accounted for by the second term in the denominator, defined as

$$C_1 = \frac{\dfrac{1}{A_{col}} \displaystyle\int_A \varepsilon_G u_{Gd} dA_{col}}{\langle \varepsilon_G \rangle U_m} . \tag{2.25}$$

The effects of nonuniform flow and phase concentrations are included in the distribution parameter C_0, which can take on several mathematical forms. While both terms in the denominator are defined analytically, simpler expressions can be derived for fully developed flow profiles in the churn-turbulent bubbly flow and slug flow regimes. The analytical model compared well to churn-turbulent and slug flow data, inasmuch as reasonable assumptions were made where values of the key variables were unavailable in the literature. Shah and Deckwer (1983) discuss analytical expressions for u_{Gd} that may be derived from the same model assuming no bubble-bubble interaction.

A gas-liquid model advocated by Wilkinson and co-workers (Wilkinson, 1991; Wilkinson *et al.*, 1992) treats the transition to churn-turbulent flow as the addition of large bubbles to a constant number of small, homogeneous bubbles. This model assumes that the small bubble population (and thus the volume fraction $\bar{\varepsilon}_{G,small}$) increases linearly with U_G in the bubbly flow regime. At transition it is assumed that the small bubble volume fraction remains constant, and additional gas flow produces only large bubbles. Deckwer and Schumpe (1993) found that the model agreed with experimental data to within 10%, but their data invalidated the assumption of a constant small bubble population and indicated a need for improvement.

Krishna and Ellenberger (1996) modified this model by using an analogy to gas-solid fluidized beds. Their modifications were justified by empirical gas holdup data of air in water; air in liquid hydrocarbons; and helium, argon, and SF_6 in tetradecane. Vertical columns used in the tests had diameters ranging from D_{col} = 10 cm to 63 cm, beyond the lower scaleup limit of 15 cm. Using the dynamic gas disengagement method, they determined the volume fractions $\bar{\varepsilon}_{G,large}$ and $\bar{\varepsilon}_{G,small}$ of "large" and "small" bubbles in the column. They then grouped the small bubbles and liquid together into a "dense" phase and identified the large bubbles as the "dilute" phase. The key quantity in their revised model is the dense phase volume fraction, $\bar{\varepsilon}_{df}$, defined by analogy to fluidized beds as the volume fraction of small bubbles in the liquid alone, excluding the volume of large bubbles:

$$\bar{\varepsilon}_{df} \equiv \frac{\bar{\varepsilon}_G - \bar{\varepsilon}_{G,large}}{1-\bar{\varepsilon}_{G,large}} = \frac{\bar{\varepsilon}_{G,small}}{\bar{\varepsilon}_{G,small} + \bar{\varepsilon}_L}. \tag{2.26}$$

Krishna and Ellenberger found that $\bar{\varepsilon}_{df}$, not $\bar{\varepsilon}_{G,small}$, was independent of superficial gas velocity beyond the transition to turbulence. This indicates that the volume fractions of small bubbles and liquid with respect to the flow volume decreased by the same proportion with increases in U_G and $\bar{\varepsilon}_{G,large}$. Studies with a variety of frits and a gas sparger demonstrated that $\bar{\varepsilon}_{df}$ and $\bar{\varepsilon}_G$, but not $\bar{\varepsilon}_{G,large}$, were dependent on the gas distribution, with more uniform distributions at the entrance region yielding higher gas holdups. They also reported that $\bar{\varepsilon}_{df}$ increased with gas density.

Using their modified two-phase model, the bubble coalescence model of Darton *et al.* (1977), their dynamic gas disengagement data, and the empirical formulas for transition of Reilly *et al.* (1994) (Eqs. 2.22 and 2.23), Krishna and Ellenberger produced the following correlation for the large bubble volume fraction for $U_G > 0.1$ m/s:

$$\bar{\varepsilon}_{G,large} = 0.268 \frac{(U_G - U_{G,trans})^{0.58}}{D_{col}^{0.18}} \tag{2.27}$$

The correlation reflects their observation that $\bar{\varepsilon}_{G,large}$ is not affected by liquid properties, gas density, or the gas phase distribution, but is significantly affected by the column diameter. The error of Eq. 2.27 in predicting large bubble holdups was 24% on average, but much less than the

error of the original correlations by Wilkinson. Further research into analytical or semi-empirical models of gas holdup is indicated.

2.3.2. Mass Transfer Models

A model commonly used to simulate liquid mixing phenomena in a vertical bubble column is the axial dispersion model, which lumps mixing phenomena within the liquid phase into a single dispersion coefficient. The model is less than effective, however, and Degaleesan *et al.* (1997) cite the wide variety of correlations for the dispersion coefficient in the literature as evidence. Deckwer and Schumpe (1993) suggest the simulation of circulation cells within the column as an improvement over axial dispersion and similar lumped models.

Degaleesan *et al.* (1997) developed and evaluated such a bubble-column model for mass transfer that compartmentalizes the column into upflow, downflow, and end regions. This approach simulates, on a coarse scale, the liquid mixing in bubble-column reactors that is driven by radially varying gas volume fractions and turbulent eddies. Each finite volume is governed by its own set of convection and diffusion equations for the concentration of chemical species, and separate equations quantify the transfer of the species between volumes. The concentration is expressed as a function of position and three parameters: liquid velocity, gas volume fraction, and turbulent eddy diffusivity. Using a radioactive particle tracking method, these parameters were measured in churn-turbulent flow in an air-water bubble column of diameter D_{col} = 19 cm. The measured quantities were then put into the model to successfully predict the motion of dye injected at the bottom of the column. To test the usefulness of the model in scaleup situations, the values of $u_L(r)$ and eddy diffusivity from the air-water system were extrapolated to churn-turbulent conditions in a three-phase slurry bubble-column reactor (D_{col} = 46 cm) used for methanol synthesis. Nuclear densitometry measurements of the radial gas volume fraction profile in the reactor supplied the remaining input to the model. The convective diffusion model did a "fair to good job" of predicting the concentration of radioactive tracers injected into the column, and determined the recirculation rate of the liquid phase well. By comparison, axial dispersion models consistently underpredicted or overpredicted the radioactive tracer concentration. Work is continuing to substantiate the correlations used in the scaleup from laboratory to industrial conditions.

2.3.3. Phase Velocity Models

Beginning with the steady-state equations of motion for a gas-liquid flow of infinite height, Ueyama and Miyauchi (1979) solved for the liquid velocity radial profile, $u_L(r)$, and cross-sectionally-averaged relative velocity, $\langle u_r \rangle$, in a cylindrical bubble column, for both "batch mode" (no net liquid flow) and a recirculating flow. For the shear stress term, the derivation assumes that the turbulent kinematic viscosity, ν_t, is much larger than the molecular kinematic viscosity, ν_{mol}, everywhere except near the column wall. The law of the wall is used in the boundary conditions, and a gas volume fraction profile of the following form is assumed:

$$\frac{\varepsilon_G(r)}{\bar{\varepsilon}_G} = \frac{n+2}{n}\left[1-\left(\frac{r}{R_{col}}\right)^n\right]. \tag{2.28}$$

The end results include a complex expression for $u_L(r)$ and an example result for $\langle u_r \rangle$ for the case of $n = 2$. Specific solutions from this model require empirical values for ν_t and an assumed value of the exponent n in the gas volume fraction profile. Experimental values of $\langle u_r \rangle$ and $u_L(r)$ from literature on recirculating bubble-column flows were in agreement with the model, but values of n were chosen based on the gas volume fraction data itself. Shah and Deckwer (1983) reported an extension of the model to a more general profile of $\varepsilon_G(r)$, and presented a previously unpublished solution for $u_L(r)$ by H. P. Riquarts based upon the same assumptions made by Miyauchi and co-workers.

Ishii and Zuber (1979) successfully developed versatile expressions for drag coefficients and drift velocities of bubbles, drops, and solid particles in a dispersed two-phase flow. They began with the two-fluid model, then applied drag similarity criteria and incorporated a mixture viscosity model. The drag similarity approach involves a relationship between the drag coefficients of a single "particle" of the dispersed phase in two extreme cases: (1) a continuous liquid medium with no other particles, and (2) a multiparticle system in which the continuous phase contains many other particles. The reference drag coefficient for the single particle-infinite medium case may be taken from any appropriate correlation for the flow of interest, and the authors have used such correlations to derive drift velocities for a matrix of dispersed phases and flow regimes. The mixture viscosity model considers not only the properties of the dispersed and continuous phases, but also the resistance to particle motion caused by the presence of other nearby particles in the fluid, and is given as

$$\frac{\eta_m}{\eta_C} = \left(1-\frac{\varepsilon_D}{\varepsilon_{D,MAX}}\right)^{-2.5\varepsilon_{D,MAX}\frac{\eta_D+0.4\eta_C}{\eta_D+\eta_C}}. \tag{2.29}$$

$\varepsilon_{D,MAX}$ is the volume fraction of the dispersed phase at the maximum possible packing. Ishii and Zuber suggest $\varepsilon_{D,MAX} = 0.62$ for monodisperse solid particles and 1.0 for fluid particles; although the theoretical value of $\varepsilon_{D,MAX}$ for solid spheres is 0.75, their value is based upon the maximum packing observed in practical situations. In Eq. 2.29 and the summary of drift velocity formulas which follows, the subscript C refers to the continuous phase, whereas D marks the dispersed phase of drops, bubbles or particles.

For solid or fluid "particles" in viscous flows, the recommended formula for the drift velocity of the dispersed phase is

$$u_{Dd} \cong u_{b\infty}(1-\varepsilon_D)^{2.0}\frac{\eta_C}{\eta_m}\frac{1+\psi(R_b^*)}{1+\psi(R_b^*)\left[\sqrt{1-\varepsilon_D}\frac{\eta_C}{\eta_m}\right]^{6/7}}, \tag{2.30}$$

where

$$\psi(R_b^*) = 0.55\left[(1+0.08R_b^{*3})^{4/7} - 1\right]^{0.75}, \tag{2.31}$$

the nondimensionalized radius of the "particle" is given by

$$R_b^* = R_b\left(\frac{\rho_C g|\rho_C - \rho_D|}{\eta_C^2}\right)^{1/3}, \tag{2.32}$$

the terminal velocity, $u_{b\infty}$, is described by

$$u_{b\infty}|u_{b\infty}| = \frac{8}{3}\frac{R_b}{C_D\rho_C}(\rho_C - \rho_D)g, \tag{2.33}$$

and the drag coefficient, C_D, is computed from an appropriate drag correlation for a single particle in an infinite medium at the corresponding Reynolds number. For solid particles at higher Reynolds numbers, which occur at $R_b^* \geq 34.65$, Eq. 2.30 simplifies to

$$u_{Dd} = u_{b\infty}(1-\varepsilon_D)^{2.0}\frac{\eta_C}{\eta_m}\frac{18.67}{1+17.67\left[\sqrt{1-\varepsilon_D}\frac{\eta_C}{\eta_m}\right]^{6/7}}. \tag{2.34}$$

For liquid drops or gas bubbles at higher Reynolds numbers, two formulas are derived. The first is for flow regimes in which the "particle" distorts and turbulent eddies influence its motion. Since the drag coefficient on the particle no longer depends upon viscosity, the formulas for terminal velocity and drift velocity simplify to produce

$$u_{Dd} \cong u_{b\infty}(1-\varepsilon_D)^n, n = \begin{cases} 1.75, \eta_C >> \eta_D \\ 2, \eta_c \approx \eta_D \\ 2.25, \eta_C << \eta_D \end{cases}, \tag{2.35}$$

where the magnitude of the terminal velocity is given by

$$|u_{b\infty}| = \sqrt{2}\left(\frac{g\sigma_s|\rho_C - \rho_D|}{\rho_C^2}\right)^{1/4}, \tag{2.36}$$

and the sign of $u_{b\infty}$ depends upon the sign of the density difference $\rho_C - \rho_D$ (*i.e.*, whether the particle rises or falls). Equation 2.35 is applicable above the following viscosity number:

$$\frac{\eta_C}{\left(\rho_C\sigma_s\sqrt{\sigma_s / g|\rho_C - \rho_D|}\right)^{0.5}} \geq 0.11\frac{1+\psi(R_b^*)}{\left[\psi(R_b^*)\right]^{8/3}}. \tag{2.37}$$

The second formula for a dispersed fluid phase applies to fully churn-turbulent flow, where "particles" can influence one another directly. In this instance the effective drag coefficient for droplets or cap bubbles simplifies further, and a force balance yields

$$|u_{b\infty}| = C\left(\frac{g\sigma_s|\rho_C - \rho_D|}{\rho_C^2}\right)^{1/4}\left(\frac{\rho_C - \rho_D}{|\rho_C - \rho_D|}\right)(1-\varepsilon_D)^{1/4}, \tag{2.38}$$

with $C = \sqrt{2}$ for bubbles and $\pi/2$ for droplets.

These velocity formulas compared satisfactorily to data and empirical correlations for flows with many different dispersed phases, including solid particles, liquid drops, bubbles, foams, and liquid-liquid dispersions. Agreement with measured data was particularly good for low dispersed-phase volume fractions. The authors considered these results to support both the drag similarity method and the mixture viscosity model.

Finally, Kumar *et al.* (1994) addressed the biggest difficulty with the two-fluid model: the Reynolds shear stress term has not yet been accurately modeled or predicted in either laboratory or industrial flow scales, making the scaleup of laboratory results difficult. Many versions of the one-dimensional bubble-column equations have been developed with different models for the shear stress term, τ_{rz}, but no model has successfully recreated all velocity or gas volume fraction data. Usually an expression is obtained for τ_{rz} in terms of ν_t, the turbulent kinematic viscosity, or l_P, Prandtl's mixing length scale (see also White, 1991):

$$\tau_{rz} = -\rho_L \nu_t\left(\frac{du_L}{dr}\right) = -\rho_L l_P^2\left(\frac{du_L}{dr}\right)\left|\frac{du_L}{dr}\right|. \tag{2.39}$$

In both expressions, du_L/dr is the radial gradient of the liquid axial velocity. The quality of fits to experimental data on u_L is sensitive to the model chosen for these quantities, particularly the model for l_P. Kumar and co-authors began with the expression for shear stress involving l_P, based on the fact that shear stress and velocity gradients can be derived from experimental measurements. Their goal was to use experimental data to determine the behavior of the mixing length scale and thus predict the effects of scaleup on bubble-column hydrodynamics.

Experimental measurements were made of the local gas volume fraction distribution, $\varepsilon_G(r,\theta,z)$, and local axial liquid velocity profile, $u_L(r,\theta,z)$, in vertical columns of five different diameters using radioactive particle tracking and tomographic techniques. Radial profiles of the Prandtl length scales of the flow were computed for one of the columns (D_{col} = 19 cm), and these $l_P(r)$ profiles were used with the one-dimensional model and the $\varepsilon_G(r)$ profiles to predict $u_L(r)$ in all five columns. The predicted and measured liquid velocity profiles were in close agreement for all columns greater than 15 cm in diameter. As expected, the model results for smaller columns deviated from the measured data because of the presence of slug flow instead of churn-turbulent flow in the column. The use of data from the 19-cm column to create valid correlations for larger columns was evidence that scaleup of velocity profiles is possible.

Because disparate values of U_G and D_{col} were used, no trends in l_P were evident, and a universal correlation for the mixing length was not reported. It was suggested that such a correlation or parametric model for conditions ranging from experimental to prototype columns would improve the accuracy of the one-dimensional, two-fluid model.

2.4. Reactor Design and Scaleup Issues

While the experiments and the analytical and semi-empirical models described in this chapter were intended to advance the body of knowledge on bubble-column reactors and multiphase flows in general, more must be learned to improve reactor design and scaleup from test conditions to operating conditions. On the experimental side, scaleup is made difficult by the lack of data taken under industrial conditions. Relatively few experiments have been conducted at elevated temperatures and pressures, although the works of Zou *et al.* (1988) and Lin *et al.* (1998) have addressed this issue. On the analytical side, challenges remain in developing scaleup models based on physics instead of experimental correlations and "know-how." For instance, Kumar *et al.* (1994) mention in passing that a two-dimensional model derived from the full two-fluid model exists, but that analytical and numerical solutions are not yet practical. The difficulty of modeling shear stress in the two-fluid model, even in its simplification to the one-dimensional two-phase model, is another example. Mathematical modeling of the three-dimensional flow also suffers from the fact that gas volume fraction profiles, which strongly influence circulation and chemical reaction rates, have yet to be determined analytically and so must be provided by experimental observation.

In the review by Deckwer and Schumpe (1993) of bubble-column design tools, a conceptual list is presented of phenomena known to influence bubble-column operation (see Figure 2.3). In particular, hydrodynamics, heat transfer, and mass transfer are identified as the scale-dependent properties that pose problems in the application of experimental data to design work. As solutions, the gas holdup correlation of Akita and Yoshida (1973), Eq. 2.11, and the mass transfer correlation of Öztürk *et al.* (1987), Eq. 2.16, are recommended for conservative design use; note, however, that the column diameter used in the latter study was less than 15 cm. Reaction kinetics and the number of reactive species (not the same as the number of phases) are mentioned as factors that can easily be included in mathematical models but have rarely been studied experimentally.

On the other hand, dimensional effects have been extensively studied. As discussed earlier, the common observation that gas holdup is insensitive to column dimensions when D_{col} > 15 cm and $(H_{col} / D_{col}) > 5$ has provided a lower limit for scaleup studies of the effects of gas flow on other quantities. The same insensitivity does not hold, however, for radial gas volume fraction profiles (Kumar *et al.*, 1997) or the bubble-size distribution (Krishna and Ellenberger, 1996). Column size is also believed to influence the liquid mixing scales, which in turn may influence reaction rates. From their model for $u_L(r)$, Ueyama and Miyauchi (1979) deduced that the turbulent kinematic viscosity, which is related to the mixing scale by Eq. 2.39, would increase as $D_{col}^{1.5}$ or a higher power, but the dependence had not yet been confirmed for large

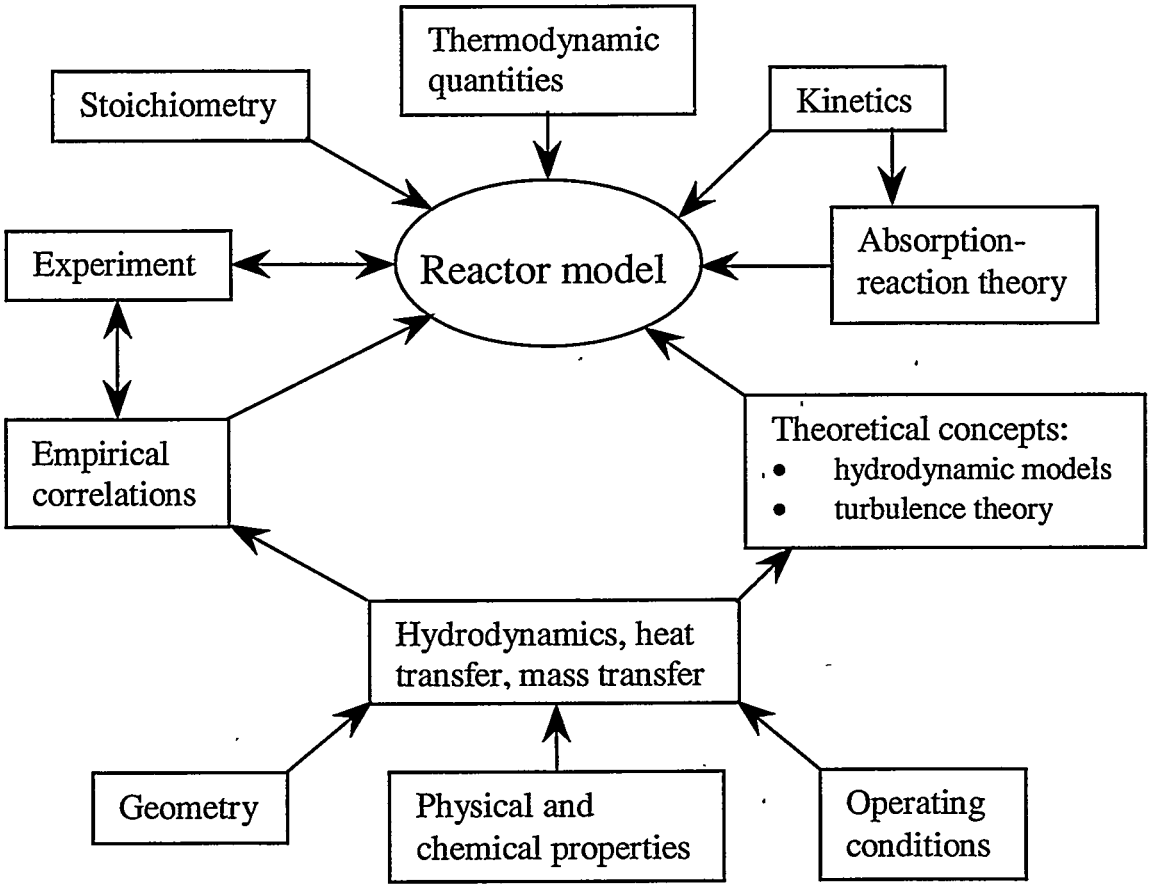

Figure 2.3. Conceptual diagram of the modeling process for bubble-column reactors. Adapted from Deckwer and Schumpe (1993).

columns. The work of Kumar *et al.* (1994) indicates that mixing effects can be scaled from small to large columns, once their dependence on other conditions is determined.

On the subject of mixing, Deckwer and Schumpe (1993) state that liquid mixing has little effect on reaction rates or reactor performance and that gas mixing, which does influence performance, is hard to quantify and therefore to predict. They recommend further studies of gas phase structures, bubble rise velocities, and related gas phase hydrodynamics. This points to the most serious deficiency in current experimental studies of bubble-column flows: measurements are typically made of time-averaged, volume-averaged quantities under the assumption that the flow field is steady-state and one-dimensional in the axial direction. Bubble-column reactors and fluidized beds are known to have three-dimensional, dynamic flow structures, but because most instrumentation is limited to measurements of average quantities, these multidimensional instantaneous flow structures are lost. Methods must be developed that can provide the instantaneous flow field information needed to characterize dynamic structures and gas mixing.

The last issue that must be addressed for successful bubble-column design is the lack of information for solid phases in multiphase flows. Fluidized beds involve a "dense phase" of solid particles, and many chemical processes involve a powdered catalyst suspended in a liquid

hydrocarbon; this makes knowledge of the effects of solid properties on mass transfer and phase distributions desirable. Unfortunately, practical models of multiphase flows involving a solid phase are scarce, although the model by Ishii and Zuber (1979) includes drift velocities for solid particles in viscous and inviscid flows. A review by Wilkinson *et al.* (1992) of experimental work in the literature concluded that the addition of solids to a gas-liquid flow increases bubble size and decreases gas holdup slightly, all else being equal.

Daly (1990) conducted experiments in two slurry bubble-column reactors of diameters 5 and 21 cm using iron oxide and silica powders, molten wax, and nitrogen gas as the solid, liquid, and gas phases, respectively. Solid volume fraction axial profiles were measured for column-averaged solid volume fractions of up to 0.30; the axial profiles were found to be uniform for particles 5 μm in diameter or less, but particles 20 μm in diameter or larger tended to settle and produce nonuniform axial distributions. This was counteracted by the introduction of a co-current flow in the solid/liquid slurry at a velocity larger than the terminal settling velocity of the solid phase. Several tests were conducted with a dual-source gamma densitometer with the intent to measure radial and axial volume fraction profiles of all three phases, but similarities in the gamma attenuation coefficients of the phases limited the resolution of measurements.

To address the unresolved issues of phase spatial variations and effects of solids in multiphase flows and to add to the knowledge base in these areas, the remaining chapters of this report present an investigation of radial volume fraction profiles in solid-liquid, gas-liquid, and solid-gas-liquid vertical column flows. While the experiments are conducted at ambient conditions, the column diameter (D_{col} = 19 cm) and fluid height ($H_{col} / D_{col} = 7.6$) in gas-liquid and three-phase flows are acceptable from the standpoint of scaleup. The experiments are also notable in that they mark the first application of electrical-impedance tomography to the quantitative measurement of volume fraction profiles in industrially relevant vertical multiphase flows.

3. The Sandia/Michigan Electrical-Impedance Tomography (EIT) System

The review in Chapter 2 of the current knowledge of vertical multiphase flows concluded with a discussion of the information that is lacking in experimental and analytical models. On the experimental side, instantaneous (rather than time-averaged) phase information and the influences of a solid phase on other phases in the flow are some of the data needed to improve the understanding of bubble-column reactors. On the analytical side, spatial variations in phase distributions are needed for three-dimensional flow modeling, but only one-dimensional radial phase distributions regularly appear in the literature; multidimensional measurements are extremely rare.

Electrical-impedance tomography (EIT) has been investigated in the literature for its ability to determine phase distributions in one and two dimensions, most often in a qualitative manner through phase "images." An electrical-impedance tomography system has been developed collaboratively by Sandia National Laboratories and the University of Michigan. This system is being extensively evaluated for its ability to quantitatively measure, rather than qualitatively image, phase distributions in solid-liquid, gas-liquid, and solid-gas-liquid vertical column flows. The motivation for this study is that quantitative EIT reconstructions are more useful in addressing the issues of analytical flow modeling and the effects of a solid phase. Also, EIT systems have the potential to obtain data over time scales of milliseconds, a feature that may allow EIT to obtain information on "instantaneous" flow structures that can, in turn, improve predictions of mixing and chemical reaction rates.

This chapter presents the details of the Sandia reconstruction algorithms and the Michigan EIT hardware. The development of both the hardware and software has been documented during their evolution (O'Hern *et al.*, 1995; Torczynski *et al.*, 1996a, 1997; George *et al.*, 1998a, 1998b, 1999c), but this chapter provides greater detail on the electronics and documents the reconstruction codes themselves. The chapter begins with an introduction to EIT theory, followed by a description of the EIT hardware and electronics. Next, the reconstruction algorithms are described along with the numerical and experimental tests used to validate them. The chapter concludes with the choice of electrode geometry for multiphase flow measurements, a process involving comparisons of domain reconstructions with numerical models. While the EIT system described in this chapter is not fast enough to obtain "instantaneous" data from multiphase flows, subsequent chapters will evaluate its ability to obtain accurate, quantitative phase measurements on time scales of tens of seconds to minutes, more quickly than other more common tomographic methods.

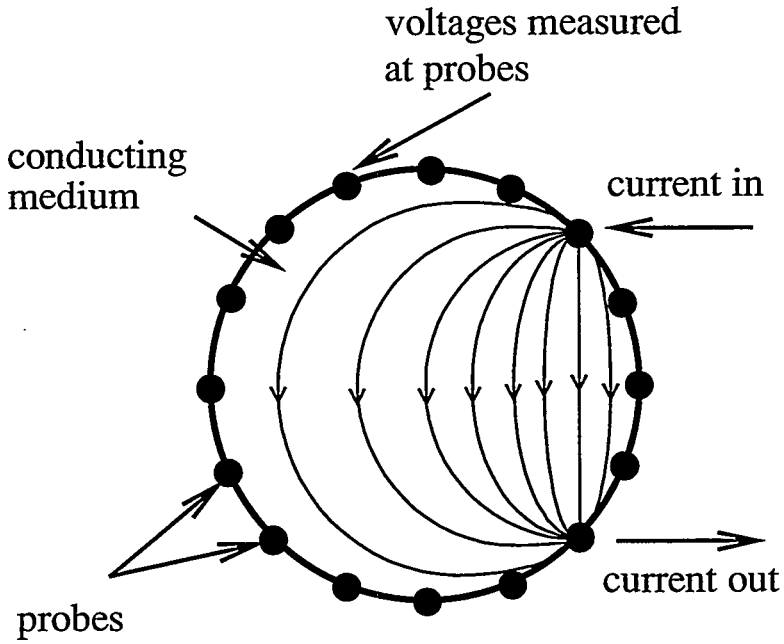

Figure 3.1. Conceptual diagram of an EIT system applied to a circular domain.

3.1. EIT Theory

In electrical-impedance tomography, a number of electrodes are mounted to the surface of a domain of interest, **D**. As a prescribed current is injected into the domain at one electrode and withdrawn at another electrode, all electrode voltages are measured relative to a reference voltage (Figure 3.1). These measurements at the domain boundary are then used to reconstruct the impedance distribution within the domain and infer the phase distribution.

Alternating current (AC) is used in EIT applications to avoid polarization effects on the electrodes. For AC electrical conduction with field frequencies on the order of tens of megahertz or lower, the electric potential within the domain, V, is related to the complex electrical conductivity of the domain, γ, by (Webster, 1990)

$$\nabla \cdot \gamma \nabla V = 0. \tag{3.1}$$

Equation 3.1 assumes that no charge sources or sinks are present in **D** and is identical in form to the steady-state heat-conduction equation. The boundary conditions on **D**, which enforce conservation of charge, are given by

$$\mathbf{n} \cdot \gamma \nabla V + q = 0, \tag{3.2}$$

where **n** is the unit normal vector outward from the domain boundary, and q is the charge flux on the boundary. Multiple measurements of q and V at the boundary of **D** are used to reconstruct

the conductivity distribution within **D**. An iterative reconstruction process is required to arrive at a conductivity distribution that will yield the measured boundary conditions. The phase distribution is then inferred from the reconstructed conductivity or impedance distribution.

In practice, current injections and voltage measurements are performed at a finite number of locations on the boundary — *i.e.*, at the electrodes — and these measurements may be averaged over a portion of the boundary surface. Consequently, the limited resolution of the reconstructed conductivity field will be strongly related to the number and locations of the electrodes used to probe the domain. If N electrodes are used, the domain can be modeled as an N-port impedance network. A prescribed current is injected into the domain at one port, known as the current source or injection electrode, and withdrawn at another port, the current sink or withdrawal electrode. The resulting voltage distribution around the "network" can be measured at $(N-1)$ ports, with one port (often the current sink) referenced to ground. The total number of linearly independent voltage measurements at the domain boundary, M, is then given by

$$M = \frac{N(N-1)}{2}. \tag{3.3}$$

M is also the number of independent impedance elements that can be determined from these voltage "projections" and used to model the domain.

To reconstruct the impedance distribution in the domain, a "candidate" impedance distribution is first constructed. A set of voltage projections is then computed from the candidate distribution. The candidate projections are compared to voltages measured on the boundary during current injection, and their difference is characterized by some error criterion. Finally, the candidate distribution is modified based on the error, and a new set of candidate projections is computed. This iterative process continues until some minimum error criterion is satisfied. Different reconstruction methods vary in the manner in which the impedance distribution is modified; the reader is referred to George (1999a) for an extensive discussion of reconstruction methods and their accuracy.

EIT reconstruction is an ill-conditioned problem. In the case of the forward problem, where a known conductivity distribution is used with Eqs. 3.1 and 3.2 to solve for voltages on the domain boundary, a single voltage solution exists for each distribution in the domain. In the inverse problem, where voltages on the boundary are used to solve for the interior conductivity distribution, such a one-to-one relationship does not generally exist. As a result, the reconstructed impedance solution may not represent a phase distribution that is physically possible or may not satisfy requirements of continuous dependence on the problem data. A more important consequence of ill conditioning is that the solution is sensitive to noise in the projections. As the number of electrodes and the spatial resolution of the solution increase, the ill-conditioning and the sensitivity to noise increase as well. When available, *a priori* information about features of the impedance distribution may be used to aid in reconstruction, as is the case for the vertical two-phase flows examined in this report.

Several simplifications are generally employed in EIT that make it possible to reconstruct the impedance distribution in the domain using discrete finite-element methods; the validity of these assumptions should be noted. First, current is commonly assumed to travel in a two-